MAGNETOHYDRODYNAMICS Vol. 42 (2006), No. 2–3, pp. 207–218

MODELING VELOCITY PULSATIONS IN A TURBULENT RECIRCULATED MELT FLOW

M. Kirpo[1], *A. Jakovičs*[1], *E. Baake*[2], *B. Nacke*[2]

[1] *Laboratory for Mathematical Modeling of Environmental and Technological Processes, University of Latvia, 8 Zeļļu Str., Rīga, LV-1002, Latvia*
[2] *Institut für Elektrothermische Prozesstechnik, Universität Hannover, 4 Wilhelm-Busch-Str., 30167 Hannover, Germany*

Turbulent recirculated flows are well known in research and industrial applications of induction furnaces and stirrers. These flows are determined by the electromagnetic Lorentz forces and usually have characteristic pulsations of velocity components, which dominate at the heat and mass exchange in the melt, especially in a zone between typical upper and lower eddies. The authors describe the results of k–ε and large eddy simulation (LES) modeling of the Wood metal flow in a cylindrical crucible for several different models. The results are compared with the experimental data.

Introduction. The induction melting is a widely used technology for the production of metals, oxides and glass. Depending on the melted material properties, different furnace types can be selected. The common feature is that in this technology an electromagnetic field generates currents and Joule heat in the material, forms a free surface and determines the flow of the melt. Under the influence of the Lorentz forces the melt flow is effectively stirred and, hence, the quality of the final product is improved. The characteristic Reynolds number $\mathrm{Re} = v_{\mathrm{ch}} \cdot l_0/\nu$ is higher than 10^4, and the stirring of the melt has a complex structure and is determined by turbulent vortices with unsteady behaviour. The turbulent flow in induction furnaces have been extensively investigated both experimentally and numerically for a long time [1], [2]. Induction furnaces usually have a symmetry axis and, therefore, most numerical simulations are 2D [3]. 2D calculations are relatively simple and usually utilize a spatially constant viscosity $\nu_{\mathrm{eff}} = \nu + \nu_{\mathrm{turb}}$ or the well-known k–ε or k–ω models. 3D calculations are performed more often since the computational power enhances [2], [4], [1]. For 3D calculations, different models can be used: 3D k–ε, LES, DNS. We have selected the LES for our 3D simulation because it is a good compromise between the computational time and the model precision.

Our previous work [5] described a simple model (Fig. 1*a*) for calculating the Wood alloy (Sn=12.5%, Pb=25.0%, Bi=50% and Cd=12.5%) melt flow in a conventional crucible. This paper describes new models of this flow and compares 2D k–ε, 3D k–ε and 3D LES simple and full models (Fig. 1*b*) with the experimental data of [6]. The results mainly describe the characteristics of the flow velocity pulsations in the melt. For industrial application, the flow fluctuations can be linked with the temperature and contaminant concentration oscillations in the melt and, hence, with the heat and mass exchange in the melt.

1. Numerical and experimental models. The experimental data are analyzed in detail in [5], [6]. The average flow consists of two dominating toroidal vortices. The momentum, heat and mass are mainly transferred from one vortex to another at low-frequency and turbulent flow velocity oscillations, which are observed in the region between the main vortices in the middle zone of the melt.

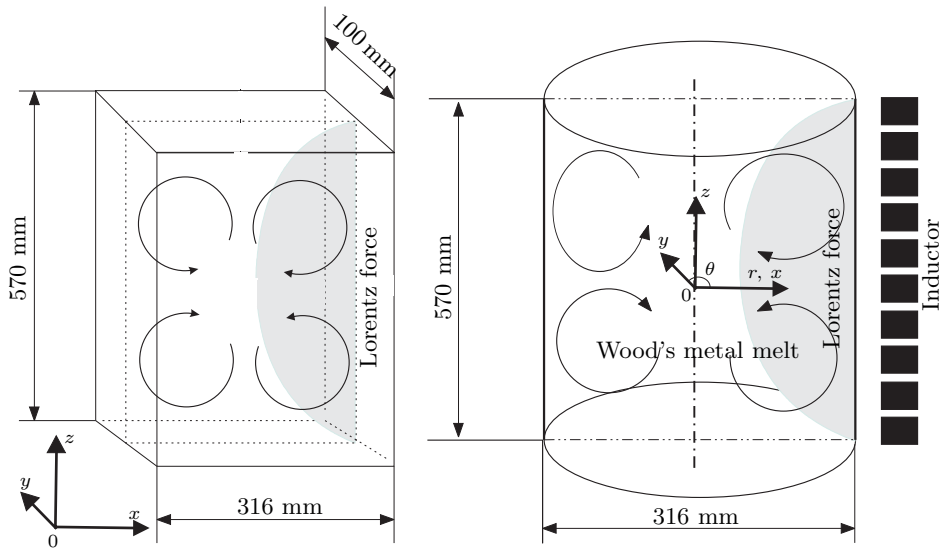

Fig. 1. (*a*) Design of the 3D simple model. (*b*) Design of the experimental crucible induction furnace and full 3D model with sketch of typical vortices of mean flow.

In a series of experiments, values of the radial and axial velocity components in the electromagnetically driven flow of the Wood metal were being measured [6] by a permanent magnet sensor (scanning rate about 20 Hz) for 60 seconds at every point of the discrete grid in a steel crucible (h = 0.57 m, D = 0.316 m). An electromagnetic field of a frequency ranged 300 to 1500 Hz was generated by a 12-coil inductor (current from 1000 A to 2200 A). A constant crucible temperature of about 80°C was kept to avoid the influence of temperature fluctuations on the flow. The filling level of the melt was varied from 50 to 120% of the inductor height, but in most of the experiments the filling level was equal to the inductor height (100%). For computer simulation, a case with 100% filling level, 396 Hz frequency and 1989 A effective current was selected.

For flow simulation, we have used the commercial finite volume code FLUENT. Mathematical description of the FLUENT k–ε and LES models can be found in [7]. The LES model is described in details in [8]. Basically, it predicts a flow of vortices, whose sizes are larger than the grid size, while smaller vortices are modeled by some sub-grid viscosity model (usually Smagorinsky).

A 2D axisymmetric electromagnetic model of the melt-crucible-inductor system was constructed in ANSYS before the flow simulation. Because our frequency is much more than 5 Hz, there is no need to consider the oscillating nature of the Lorentz forces and the tangential force component [4]. EM forces were directly transferred to every finite volume in FLUENT (transfer error is less than 1%).

Three types of geometry models were used for calculations (Table 1). All models had the same boundary layer and grid parameters. The characteristic mesh size of 3 mm is enough for our calculations because we have refined the border layer, our model has a 100 times larger diameter, and models on more coarse grids yield qualitative results [4]. The Courant number Cr = $v{\cdot}\delta t/\delta x$, where v is the mean velocity, δt and δx are the corresponding time step and mesh size, is about 0.25 in all cases, so the numerical dispersion does not influence the accuracy of solution.

Table 1. Geometry and mesh parameters.

Mesh reference	N1	N2	N3
Mesh geometry	2D plane	3D box	3D cylinder
Number of grid points (thousands)	10.6	145	1741
Typical mesh size,mm	3	3	3
First border layer, mm	0.5	0.5	0.5
Number of border layers	4	4	4
Time step, ms	–	5	5

2. Modeling results and discussion. No shear stress boundary condition was used for the top surface of the melt. All other surfaces had no slip conditions. The initial velocity field was set zero. Depending on the model, a steady or a transient analysis was performed. The LES model results provide much information and will be discussed in detail. For 3D simulations, only a transient LES model was used. The time step in the full LES model was selected to be 5 ms or 10 ms. The averaged results are almost independent on the time step. A smaller time step is more convenient for spectral analysis of calculated velocities, a larger time step can be used to get fast averaged results. 60 seconds of the flow development were calculated (Fig. 2). Calculations were performed iteratively until each variable change is less than $< 10^{-3}$.

Two parameter models (k–ε and k–ω) accurately predict the pattern of the averaged flow, which corresponds to those observed in experiments – two dominating vortices of approximately equal size and intensity (lower vortex intensity is a little larger). The smaller intensity of the upper vortex can be explained by corner effects: the inductor height is equal to the crucible filling level, but the boundary conditions at the top and near the bottom are different. The melt motion is initiated by the azimuthal component of the Lorentz force rotor: $(\mathrm{rot}\,\vec{F})_z = \partial F_z/\partial r - \partial F_r/\partial z$. The absolute value of the axial Lorentz force component in the bottom part is larger than at the top of the crucible because the geometry and $\partial F_z/\partial r$ are more crucial near the corners of the crucible.

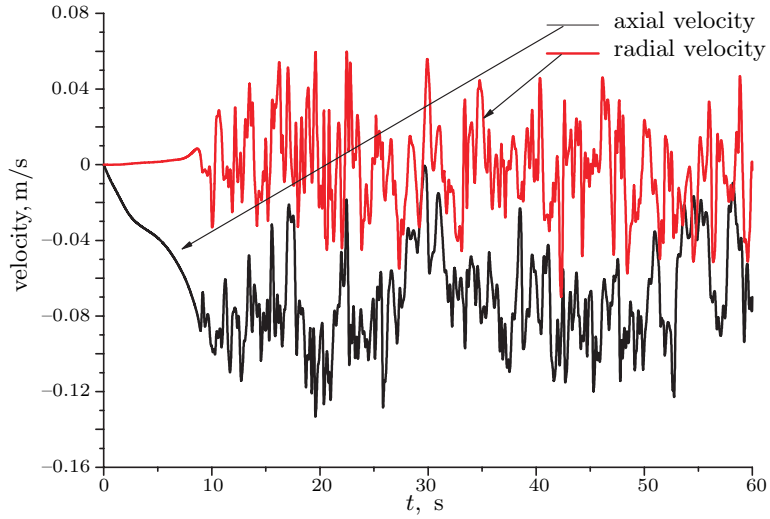

Fig. 2. N3 model instantaneous axial and radial velocity components, $r = 0$, $z = -0.21$ m ($I = 1989$ A, $f = 396$ Hz).

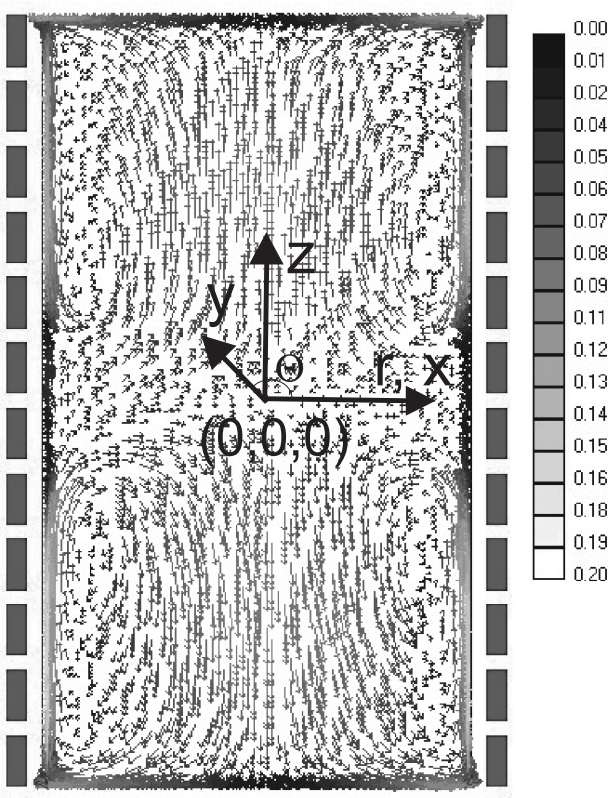

Fig. 3. N3 model averaged velocity distribution in m/s ($v_{\max} \approx 0.17\,\mathrm{m/s}$).

3D LES calculations are more accurate for the description of instantaneous turbulent quantities if compared to two-equation models. LES modeling results allow to see the flow development in time and get an averaged flow pattern (Fig. 3), which is in good accordance with experiment and 2D models. On the other hand, 3D unsteady calculations are very time consuming. By selecting the grid size and the time step, the unsteady flow can be calculated in a reasonable time, and turbulence can be modeled even in a dissipation range – it means that the energy cascade transfer is calculated directly by the LES method, if the selected time step and the grid size correspond to an appropriate Kolmogorov scale length $\lambda_d = \varepsilon^{-1/4}\,\nu^{3/4}$ ($\lambda_d \approx 10^{-4}\,\mathrm{m}$ for the flow under study).

The instantaneous velocity components exhibit a complicated frequency dependence. In first seconds of the flow, the velocity develops faster at the near-wall regions. Velocity changes at the symmetry axis are not so rapid because of the flow inertia. Approximately in 8 s, the flow regime becomes turbulent everywhere in the crucible and the velocity oscillations arise (Fig. 2).

For better comparison of the results, several characteristics lines were selected: the diameter in the xz-plane, the z-axis at $r = 0$ and the vertical line at $r = 0.15\,\mathrm{m}$. On these lines, the axial and radial velocity components were compared. The axial velocity profiles at selected time moments are illustrated in Fig. 4 on the vertical line $r = 0.15\,\mathrm{m}$, and in Fig. 5 on the diameter. These figures show how the axial velocity changes with time: instantaneous flow vortices keep the basic pattern of the flow, but vortices of smaller sizes play an important role too. Concurrent to

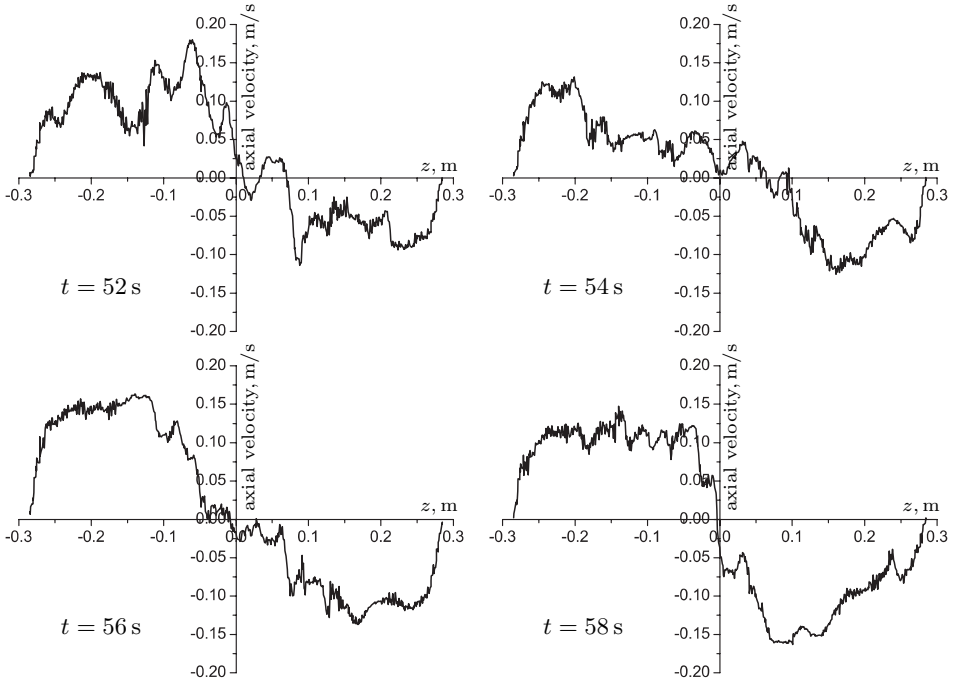

Fig. 4. N3 model calculated axial velocity in m/s at $r = 0.15$ m for time 52, 54, 56 and 58 s.

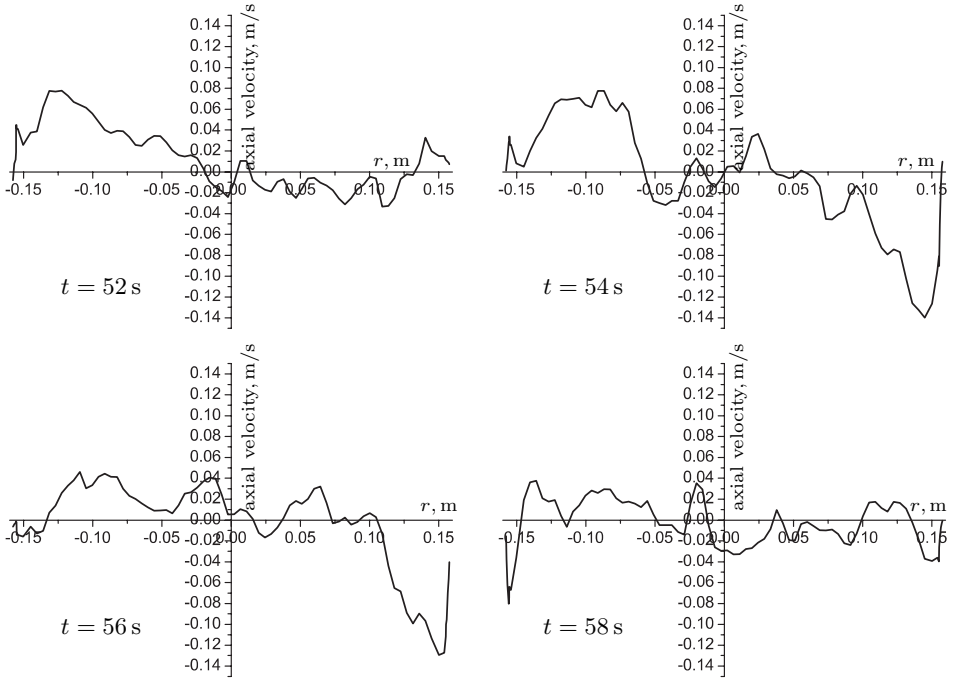

Fig. 5. N3 model calculated axial velocity in m/s at $z = 0$ for time 52, 54, 56 and 58 s.

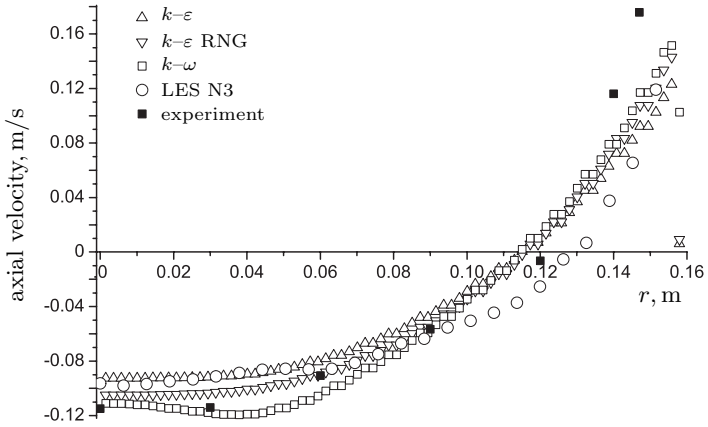

Fig. 6. Axial velocity profile at $z = -0.165\,\mathrm{m}$.

the basic vortex of the characteristic height 0.25 m, which is determined by the geometry and nature of outer (Lorentz) forces, are local vortices of characteristic scales between $0.01 \div 0.05\,\mathrm{m}$. In the middle zone of the crucible ($z = 0$), where $\partial F_r/\partial z \approx 0$, the flow is very unstable. Two opposite flow jets run parallel to the crucible wall into collision and are drawn away from the wall. The axial velocity of the averaged flow near the wall and in the geometry center must be close to zero in the ideal case ($v_z \to 0$). The radial velocity of the flow has its maximum between the near-wall region and the geometry center. In the flow under study, the axial velocity intensity oscillates along the wall under the influence of local vortices (Fig. 4). Interchanging streams of different instantaneous axial velocity intensities are observed. Vortices of different sizes are drawn away from the wall to the regions of opposite averaged vortices. In this way, the effective impulse and scalar (temperature, concentration) value transfer is ensured between the upper and the lower eddies.

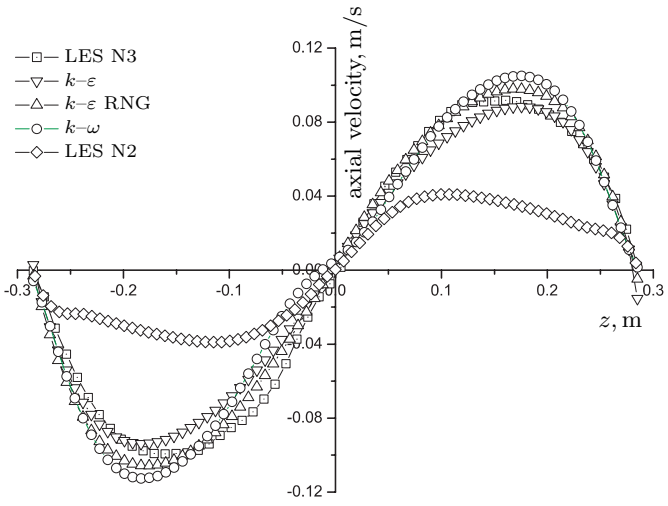

Fig. 7. Axial velocity profile at $r = 0$.

Experimental and modeling results are compared for the radius at $z = -0.165\,\mathrm{m}$ (lower vortex, Fig. 6). Experimental data are reconstructed using black boxes. The best fit is achieved using the k–ε RNG model, but all model results show good agreement with the experimental data. Some difference from the experimental results is observed in the near-wall region. There might be two reasons: computational effects and difficulties in velocity measurements in the near-wall region (geometry and EM field effects). LES N3 results are comparable with 2D model results.

Fig. 7 shows an axial velocity distribution on the symmetry axis for 2D models and averaged LES models. The LES N2 model maximum axial velocity value is smaller than in the other models because the N2 model has a rectangular form and due to the mass conservation law the flow velocity in the middle zone should be smaller than in the near-wall region (vortex centers are closer to the crucible walls). The flow regime in the N2 case is still turbulent ($\mathrm{Re} > 10^4$). Models N1 and N3 have velocity maxima approximately between the top or bottom surfaces and the center, while the N2 velocity maximum is closer to the geometry center (Fig. 7).

Velocity autocorrelation coefficients $R_{i\,i}(\tau) = \overline{v_i(\vec{r}, t)\, v_i(\vec{r}, t+\tau)}$ were computed (Fig. 8). Autocorrelation coefficients calculated from the experimental or modeling results have s similar structure. Coefficients have local maxima at

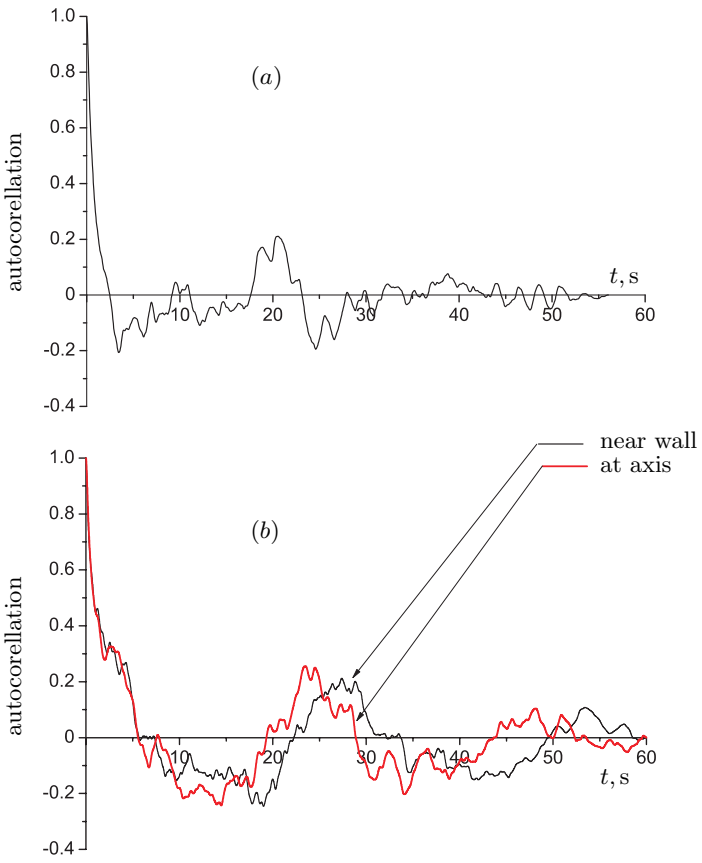

Fig. 8. (*a*) Experimental and (*b*) LES N3 calculated axial velocity autocorrelation for point on axis.

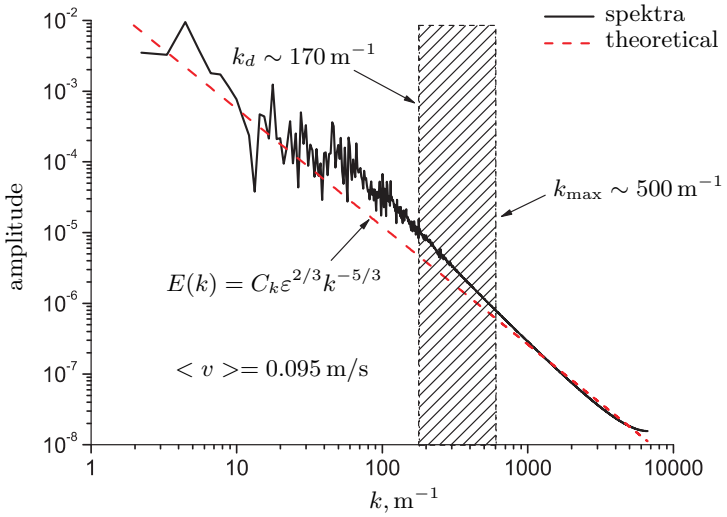

Fig. 9. Turbulent energy spectra in wave number space near the crucible wall.

$\tau \approx 20 \div 25\,\mathrm{s}$. This time step τ is approximately equal to the circumference period of fluid element in the averaged toroidal vortex $T = 2\pi R_{\mathrm{ch}}/v_{\mathrm{ch}}$. Taking an inverse Fourier transform from the autocorrelation coefficient, we can get an Eulerian time spectrum [9]:

$$\Psi_{i\,i}(\omega) = \frac{1}{2\pi} \int_{-\infty}^{\infty} \mathrm{e}^{-i\omega\tau} R_{i\,i}(\tau)\mathrm{d}\tau, \tag{1}$$

where $\omega = 2\pi f$. Such dimensional time spectrum was calculated for each velocity component. All three spectra were added together to get full energy time spectra. The experimental results contain data only for the axial and radial velocities and their spectra were multiplied by 3/2 using an isotropic turbulence approximation. However, further analysis shows that turbulence can be exposed as isotropic only in a part of the complete flow. Frequency spectra were converted into wave number spectra using a Taylor's hypothesis: $k = \omega/v$, where v is the averaged velocity at a current point (Fig. 9). Regions with a high enough averaged velocity were selected ($v \approx 0.09\,\mathrm{m/s}$).

The experimental measurement frequency was 20 Hz, and the distinction ability in space did not exceed $k_{max} \approx 500\,\mathrm{m}^{-1}$ (with 0.09 m/s average velocity). The computational time step is 5 ms, which corresponds to a 10 times better resolution. However, we must take into account the space discretization of the models with a characteristic element size of 3 mm. The numerical cut-off wave number can be estimated as $1/(2\delta x)$ [4] (for uniform mesh). In our case, the cut-off wave number k_d is about $170\,\mathrm{m}^{-1}$. Therefore, our model cannot calculate turbulent structures with scales smaller than $1/170\,\mathrm{m}$ ($\approx 0.006\,\mathrm{m}$), which are comparable with the size of the measuring part of the probe.

All spectra have several frequencies with a relatively high energy (this effect can be best noticed in Fig. 10 (left)). The computed and experimental spectra can be compared with the theoretical Kolmogorov spectrum in the inertial subrange [9]:

$$E(k) = C_k \varepsilon^{2/3} k^{-5/3}, \tag{2}$$

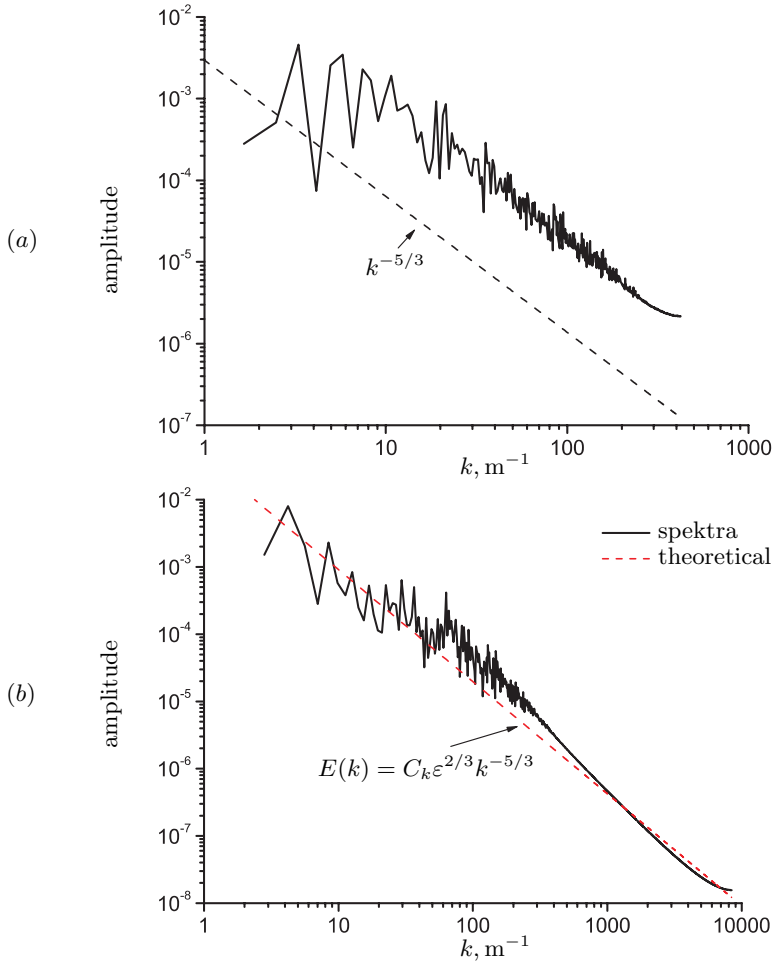

Fig. 10. (*a*) Experimental and (*b*) calculated turbulent energy spectra at symmetry axis.

where the turbulent dissipation rate ε can be computed taking the integral:

$$\varepsilon = 2\nu \int_0^{+\infty} k^2 E(k) \mathrm{d}k \tag{3}$$

from the energy spectrum $E(k)$, where $\nu = 4.5 \cdot 10^{-7}\,\mathrm{m^2 s^{-1}}$ for the melt. The theoretical Kolmogorov constant C_k is usually taken to be 1.5. Dashed lines in Figs 9 and 10 (right) represent theoretical curves calculated by these formulas. The observed zone with equal slopes corresponds to the inertial range. The inertial range is narrow because our mesh and the selected time step restrict observations of high scale oscillations. Decay of the computational curve at high k values is faster because of the subgrid viscosity and numerical effects.

Wavelet analyses were made to better realize how the velocity oscillation frequency changes in time. Fourier analyses are not localized in time, hence, it is difficult to get information about fast local variations of the analyzed signal. Wavelet analyses are performed using special functions with certain properties

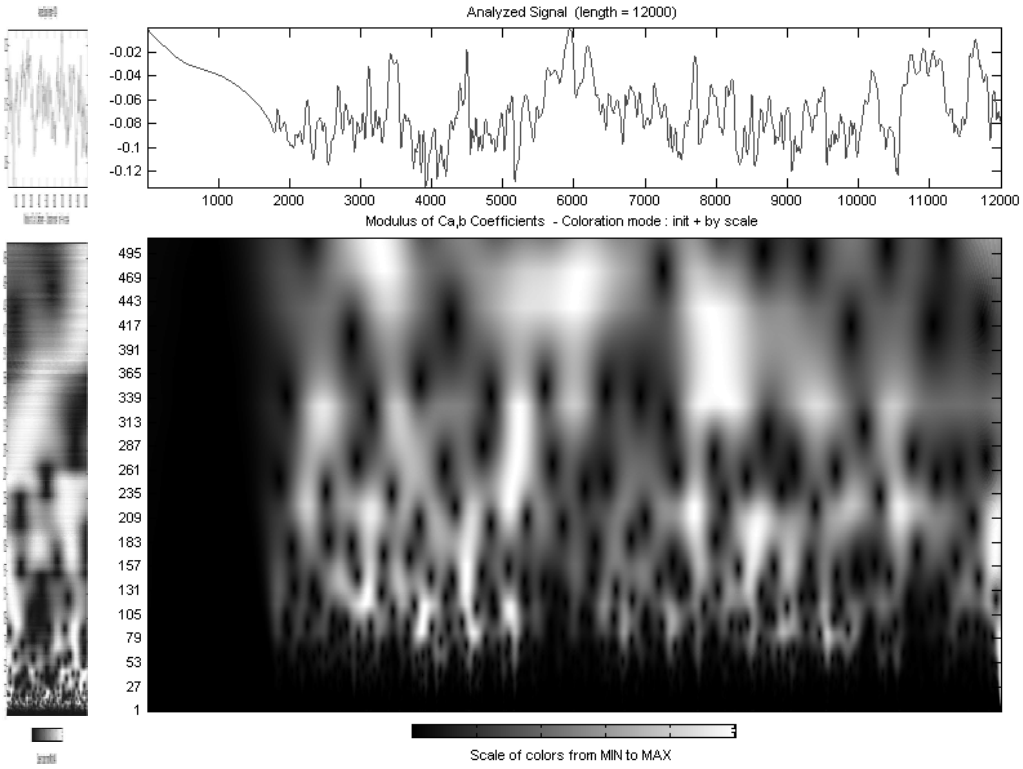

Fig. 11. Wavelet analysis of axial velocity component on symmetry axis: experimental (left) and modeling (right). Signal length is 1000 and 12000 points. Left axis represents scale.

$\Phi(a,b)$:

$$\Phi(a,b,t) = \Phi\left(\frac{t-b}{a}\right), \tag{4}$$

where coefficients a and b correspond to scale and positions. Continuous wavelet transform coefficients are expressed as:

$$C(a,b) = \int_{-\infty}^{+\infty} f(t)\Phi(a,b,t)\mathrm{d}t. \tag{5}$$

The wavelet coefficients for experimental and computational results, which are obtained using the Morlet wavelet $\Phi(t) = \frac{1}{\sqrt{\pi a}}\mathrm{e}^{2i\pi bt}\mathrm{e}^{-\frac{t^2}{a}}$, are shown in Fig. 11. Both data sets contain different number of points, but the signal length in real time is 60 s for both cases. The scale can be interpreted as a reciprocal frequency. Larger scales represent lower frequencies and vice versa. Numerical values of the frequency can be found too, but we simply want to see if there is a dominating frequency, which is more or less constant over time. Figures show that there is no dominating frequency, but there are several such frequencies. The wavelet transform of the experimental data shows the same trend as the transform of the modeled flow velocity.

Our calculation technique makes possible an anisotropy analysis of the flow. Flow anisotropy can be studied in different ways using different reference values.

Table 2. Relative strength of velocity gradients in different directions.

Point	$G_{xx,yx}$	$G_{xx,zx}$	$G_{xy,yy}$	$G_{xz,zz}$	$G_{xy,zy}$	$G_{xz,yz}$
isotropic [10]	0.5	0.5	2	2	1	1
$r = 0$, $z = 0$	6.4	24.9	1.2	1.5	4.7	1.2

We have selected coefficients $G_{ij,kl}$ as an anisotropy measure [10]:

$$G_{ij,kl} = \frac{\langle(\partial u_j/\partial x_i)^2\rangle}{\langle(\partial u_l/\partial x_k)^2\rangle},\ i,j,k,l = x,y,z. \tag{6}$$

Calculations should be performed with fluctuations (averages are removed) [11] for correct analysis. We have selected a point in the center of the crucible (on the symmetry axis between the upper and lower averaged vortices), where the average velocity is zero and the anisotropy analysis can be made directly on velocity gradients. Illustrative values are presented in Table 2, where they can be compared with theoretical values for isotropic turbulence [10]. As can be seen, the recirculated flow in the crucible exhibits the turbulence anisotropy. Coefficient values in other parts of the flow are even larger, so we can conclude that isotropic laws cannot be applied to such types of flows.

Conclusions. The LES model is proved to be a very good tool to make statistical analysis of the turbulent flows. Turbulent flow modeling limitations are mainly related to the mesh size and time step selection. Disadvantages of the LES method can be a long computational time and a sizeable amount of results for post-processing. The LES model averaged flow has the same characteristics as the measured mean flow and the 2D calculated mean flow. Wavenumber space experimental and computational spectra are in accordance with the Kolmogorov theory. According to our transient analysis, pulsating velocities show several dominating frequencies, which are not time localized, but can vary from one to another. Further work can include acquisition of new experimental data.

Acknowledgements. This paper has been supported by the *European Social Fund (ESF).*

REFERENCES

[1] E. Baake, B. Nacke, A. Umbrashko, A. Jakovics. Large eddy simulation modeling of heat and mass transfer in turbulent recirculated flows. *Magnetohydrodynamics*, vol. 39 (2003), no. 3, pp. 291-298.

[2] R. Schwarze, F. Obermeier Modelling of unsteady electromagnetically driven recirculating melt flows *Modelling Simul. Mater. Sci. Eng.*, vol. 12 (2004), pp. 985–993.

[3] A. Bojarevics, V. Bojarevics, Yu.M. Gelfgat, K. Pericleous. Liquid metal turbulent flow dynamics in a cylindrical container with free surface: experiment and numerical analysis. *Magnetohydrodynamics*, vol. 35 (1999), no. 3, pp. 205–222.

[4] F. Felten, Y. Fautrelle, Y. Du Terrail, O. Metais. Numerical modelling of electromagnetically-driven turbulent flows using LES methods. *Applied Mathematical Modelling*, vol. 28 (2004), pp. 15–27.

[5] M. Kirpo, A. Jakovics, E. Baake. Characteristics of velocity pulsations in a turbulent recirculated melt flow. *Magnetohydrodynamics*, vol. 41 (2005), no. 2, pp. 199–210.

[6] E. Baake. *Grenzleistungs- und Aufkohlungsverhalten von Induktions-Tiegelöfen* (VDI, Düsseldorf, 1994.)

[7] Fluent 6.2 Users's Guide, 2005.

[8] P. Sagaut. *Large Eddy Simulation for Incompressible Flows*, 2nd edition. (Springer, 2002.)

[9] H. Tennekes, J.L. Lumley. *A First Course in Turbulence.* (The MIT Press, London, 1972.)

[10] B.S. Pope. *Turbulent Flows.* (Cambridge University Press, 2000.)

[11] W.D. Smyth, J.N. Moum Anisotropy of turbulence in stably stratified mixing layers *Phys. Fluids.*, vol. 12, issue 6, pp. 1343–1362.

Received 17.03.2006